

# Quantum interference in the quasi-one-dimensional organic conductor $(\text{Per})_2\text{Au}(\text{mnt})_2$

D. Graf,<sup>1</sup> J. S. Brooks,<sup>1</sup> E. S. Choi,<sup>1</sup> M. Almeida,<sup>2</sup> R. T. Henriques,<sup>2</sup> J. C. Dias,<sup>2</sup> and S. Uji<sup>3</sup>

<sup>1</sup>National High Magnetic Field Laboratory and Department of Physics, Florida State University, Tallahassee, Florida 32310, USA

<sup>2</sup>Instituto Tecnológico e Nuclear/CFMUL, Estrada Nacional No. 10, P-2686-953 Sacavém, Portugal

<sup>3</sup>National Institute for Materials Science, Tsukuba, Ibaraki 305-0003, Japan

(Received 18 February 2007; revised manuscript received 19 March 2007; published 1 June 2007)

The quantum interference (QI) of charge carriers in a magnetic field is obtained in the organic conductor  $(\text{Per})_2\text{Au}(\text{mnt})_2$  by suppressing the charge-density-wave (CDW) state with pressure. The QI oscillation amplitude exhibits a temperature-dependent scattering rate, indicative of an inhomogeneous metal-CDW ground state. The QI oscillation frequency reveals a Fermi-surface topology in close agreement with band-structure predictions. The value of the frequency is quite small, making the limit of constructive interference experimentally accessible.

DOI: 10.1103/PhysRevB.75.245101

PACS number(s): 72.15.Nj, 71.20.Rv

## I. INTRODUCTION

The interference of electrons, first realized in the diffraction pattern of electrons incident on nickel,<sup>1</sup> has been observed in electrostatic bi-prism experiments<sup>2</sup> and in a double-slit arrangement analogous to Young's optical interference experiment.<sup>3</sup> In a magnetic field the relative phases of interfering electron beams can be controlled,<sup>4,5</sup> and the effects of magnetic flux on the quantum states of charged particles are now well understood.<sup>6</sup> In a metal, the effect involves the interference of two electron trajectories on different Fermi-surface (FS) sections, with a phase difference of  $\Psi = 2\pi\phi/\phi_0$  (see Fig. 1). Here  $\phi/\phi_0$  is the ratio of the magnetic flux enclosed between the electron paths to the magnetic flux quantum  $h/e$ . Scattering between carrier trajectories involves the "Stark" interference effect,<sup>7,8</sup> where carriers either tunnel through (magnetic breakdown) or reflect (Bragg scatter) from loop vertices. An oscillatory magnetoresistance (MR) signal, periodic in inverse field, is present in electrical transport measurements. But as discussed below, MR oscillations observed due to quantum interference (QI) are distinct from the Shubnikov-de Haas (SdH) oscillations associated with closed orbits and Landau quantization (LQ). QI effects have been previously observed in organic,<sup>9</sup> inorganic-elemental,<sup>7</sup> and compound metals<sup>10</sup> where quasi-two-dimensional or three-dimensional electronic structures allow coexisting (competing) SdH and QI oscillations. The situation is simplified in quasi-one-dimensional metals, as is the case for several of the Bechgaard salts<sup>11-14</sup> where pairs of open-orbit Fermi-surface sheets at  $\pm k_F$  similar in form to the case shown in Fig. 1, can occur.

In this paper we describe the QI phenomenon in the quasi-one-dimensional organic metal<sup>15</sup>  $(\text{Per})_2\text{Au}(\text{mnt})_2$  where the application of pressure suppresses the charge-density-wave (CDW) ground state below the transition temperature  $T_{\text{CDW}} = 12$  K.<sup>16</sup> This work is motivated by the complex, magnetic-field direction-dependent MR behavior of the CDW ground states in both  $(\text{Per})_2\text{Au}(\text{mnt})_2$  (Ref. 17) and  $(\text{Per})_2\text{Pt}(\text{mnt})_2$  (Ref. 18). By suppressing the CDW behavior, the topology of the unnested Fermi surface, as recently computed by Canadell, Almeida, and Brooks<sup>19</sup> and schematically shown in Fig. 1, can be accessed through magnetotransport measurements.

## II. EXPERIMENTAL DETAILS

Single crystals of  $(\text{Per})_2\text{Au}(\text{mnt})_2$  were prepared electrochemically<sup>20</sup> with sample sizes of approximately  $1 \text{ mm} \times 20 \mu\text{m} \times 10 \mu\text{m}$  in the respective  $b$ ,  $a$ , and  $c$  crystallographic directions. Here  $12\text{-}\mu\text{m}$  gold wires were attached to each sample along the conducting chain ( $b$ -axis) direction. In all cases the four-terminal resistance was measured along the  $b$  axis using standard low-frequency ac lock-in methods. In making these measurements, careful checks of nonlinearity were made by varying the current between  $0.1$  and  $100 \mu\text{A}$  (corresponding to electric fields between  $1 \mu\text{V}/\text{cm}$  to  $1 \text{ mV}/\text{cm}$ ).<sup>21</sup> Previous threshold field estimates made at ambient pressure<sup>22,23</sup> do not provide relevant information for comparison with our results since the resistance under pressure is dramatically lower [see Fig. 2(a)]. A more appropriate comparison is with the nonlinear response found by Mitsu *et al.*<sup>16</sup> for the compound under pressure, as shown in Figs. 4 and 5 of Ref. 16. Here a departure is seen from Ohmic behavior above  $\sim 5 \text{ mV}/\text{cm}$ . Hence, our currents and electric fields (corresponding to  $10 \mu\text{A}$  and  $0.1 \text{ mV}/\text{cm}$ , for example) were well into the linear response regime in all cases.

Hydrostatic pressure was achieved by either conventional clamp-type cells using Daphne oil 7373 as the medium or

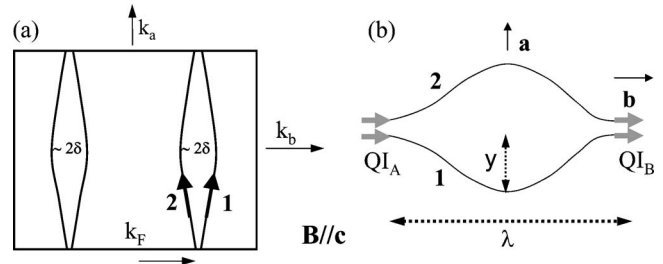


FIG. 1. (a) Simplified Q1D Fermi surface for  $(\text{Per})_2\text{Au}(\text{mnt})_2$  (after Ref. 19). The lattice parameters and bandwidths are  $(a, b, c) = (16.6, 4.19, 26.6) \text{ \AA}$  and  $(t_a, t_b, t_c) \sim (2, 150, < 0.1) \text{ meV}$ , respectively (Ref. 19);  $k_F = 0.56 \text{ \AA}^{-1} \pm \delta$ ,  $\delta \sim 0.002k_b$ , and  $v_F \sim 1.6 \times 10^5 \text{ m/s}$ . (b) Real-space motion of the carriers with wavelength  $\lambda = 2\pi\hbar/eBa \sim 2.5/B$  ( $\mu\text{m T}$ ) and amplitude  $y = 4t_a/e v_F B \sim 50/B$  ( $\text{nm T}$ ). Transmission or reflection of the carriers can occur at the interference nodes  $QI_A$  and  $QI_B$ .

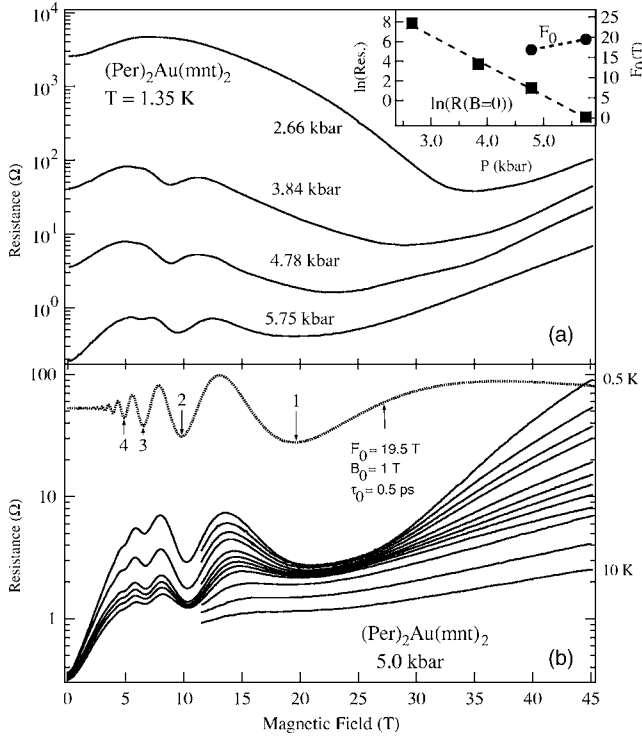


FIG. 2. Pressure, temperature, and magnetic field dependence of the resistance of  $(\text{Per})_2\text{Au}(\text{mnt})_2$  for  $B\parallel c$  and  $I\parallel b$ . (a) Magnetic-field-dependent resistance for different helium gas pressures at 1.35 K for sample PA1. Inset: pressure dependence of zero-field resistance and oscillation frequency  $F_0$ . (b) Temperature dependence of the MR of sample PA2 at 5 kbar between 0.5 and 10 K, where the intermediate temperatures are 0.8, 1.10, 1.35, 2.0, 2.5, 3.0, 3.5, 4.3, 6.0, and 8.0 K. Inset: QI oscillatory term  $-2pq \cos(\Psi)\exp(-\pi/\omega_c\tau)$  for representative parameters. Indices  $N=1, 2, 3$ , etc., are for  $\Psi=N2\pi$ . (See text for discussion.)

with a helium-gas pressure cell. Pressures for the clamp cell were corrected for pressure loss when cooled from room temperature.<sup>24</sup> The pressure cells were immersed in either  $^3\text{He}$  or  $^4\text{He}$  during low-temperature measurements, and superconducting (18 T), resistive (33 T), and hybrid (45 T) magnets were used at various stages of the investigation.

### III. RESULTS AND DISCUSSION

The pressure (helium gas) and magnetic field dependence of the resistance of  $(\text{Per})_2\text{Au}(\text{mnt})_2$  (sample PA1) at 1.35 K is shown in Fig. 2(a). The MR evolves from the ambient-pressure high-resistance behavior associated with the CDW state<sup>17</sup> to a low-resistance state where oscillations periodic in  $1/B$  emerge. At low temperatures, the  $B=0$  resistance decreases exponentially with pressure, and the frequency ( $F_0$ ) of the oscillations increases [inset of Fig. 2(a)]. In Fig. 2(b), for sample PA2 in a clamp cell at 5 kbar, the temperature dependence of the oscillatory behavior is presented. Dips in the oscillatory MR indexed versus inverse field yield an oscillation frequency of  $F_0=19.5$  T. A fast Fourier transform (FFT) for a magnetoresistance trace observed at  $T=0.5$  K is shown in Fig. 3. Though the FFT does show a frequency of

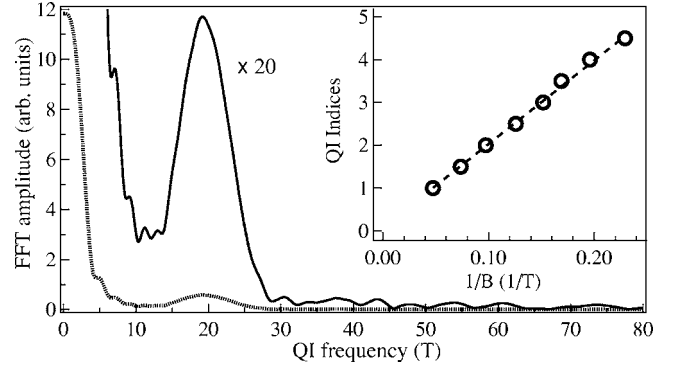


FIG. 3. Fast Fourier transform spectrum of the  $T=0.5$  K data in Fig. 2(b) (dotted line) with a peak at 19.2 T. The same FFT is expanded for clarity (solid line). Inset: peak and valley index vs inverse field location, which gives a frequency from the slope (dashed line) of 19.7 T.

$\sim 20$  T, we normally used the peak and valley positions in  $1/B$  to calculate the frequencies. In general, the FFT was less reliable due to the small number of oscillations, especially at higher temperatures. The inset to Fig. 3 shows the index of the quantum interference peak plotted against inverse field location, where a linear fit agrees well with the FFT value.

Although the oscillations are reminiscent of the SdH effect, we argue below that LQ cannot lead to the quantum oscillatory effects observed in pressurized  $(\text{Per})_2\text{Au}(\text{mnt})_2$ ; rather, the system is acting as a quantum interferometer. This assertion is supported by the significant difference between the LQ and QI behaviors in terms of the temperature and field dependences of the oscillation amplitudes:

(i) *Landau quantization.* For LQ, the product of three Lifshitz-Kosevich (LK) reduction factors determines the oscillation amplitude for a quasi-two-dimensional (Q2D) cylindrical system:<sup>25</sup>  $R_T=X/\sinh(X)$ ,  $R_D=\exp(-X_D)$ , and  $R_S(r)=\cos(|\pi r g m_c(\theta=0)/2 \cos(\theta)|)$ . Here,  $X=\alpha m_c T/B$  (for  $X_D$ ,  $T$  is replaced with the Dingle temperature  $T_D=\hbar/2\pi k_B\tau$ , where  $\tau$  is the scattering time),  $\alpha=2\pi^2 k_B m_c / e\hbar$ ,  $r$  is the harmonic number,  $g$  is the Landé factor,  $m_c$  is the cyclotron effective mass normalized by the bare electron mass ( $m_e$ ), and  $\theta$  is the angle between the applied magnetic field and the axis of the Q2D cylinder.  $R_T$  takes into account the effects of finite temperature which broaden the Fermi distribution at the Fermi surface. Oscillations are further affected by  $R_D$  and  $R_S$  due to the carrier lifetime and Zeeman splitting of the Landau levels, respectively. Neglecting the physical constants and  $R_S$ , the field and temperature dependence of the LQ oscillation amplitudes is  $A_{LQ}=R_T R_D \sim (m_c T/B)/\sinh(m_c T/B)\exp(-1/\tau B)$ .

(ii) *Quantum interference.* In contrast to LQ, the amplitudes of QI oscillations will depend on the magnetic breakdown ( $p$ ) and Bragg reflection ( $q$ ) probabilities of the carriers at interference nodes (labeled  $\text{QI}_A$  and  $\text{QI}_B$  in Fig. 1), which are  $p=\exp(-B_0/B)$  and  $q=(1-p)$ .<sup>14,25</sup> Here  $B_0\sim m^* E_g^2 / \hbar e E_F$  is the magnetic breakdown field where  $E_g$  is the energy gap between bands 1 and 2 and  $m^*$  is the effective mass. For the simple topology in Fig. 1, the total QI transmission probability<sup>14,25</sup> will be  $\sim p^2+q^2-2pq \cos(\Psi)$ . The temperature dependence of the QI oscillation amplitude only

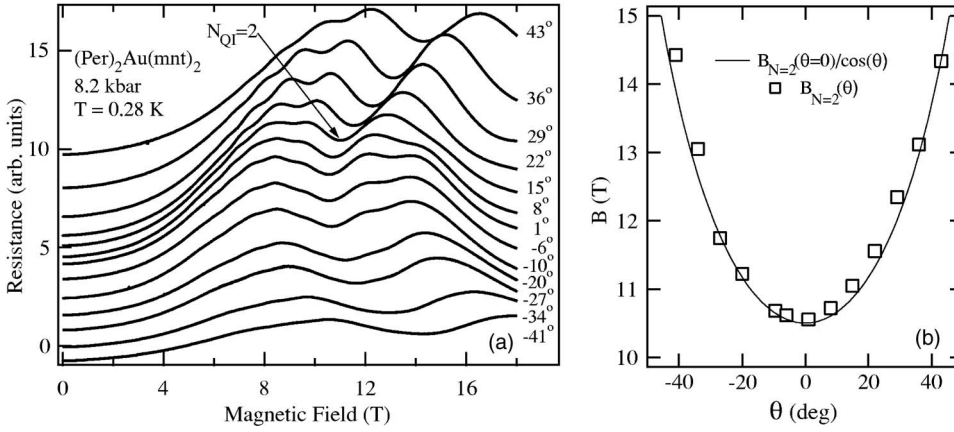


FIG. 4. Angular dependence of MR oscillations in  $(\text{Per})_2\text{Au}(\text{mnt})_2$  (sample PA2) at 8.2 kbar and 0.28 K. The curves are offset for clarity.  $\theta=0$  is defined as the orientation where oscillatory features appear at the lowest field. (b) Field position of the  $N=2$  dip feature vs  $\theta$ .

depends on the carrier lifetime  $\tau$  between QI nodes, which causes an attenuation of the form<sup>26</sup>  $\exp(-\pi/\omega_c\tau)$ . Here, for a Q1D system, the cyclotron frequency  $\omega_c = eBv_F/\hbar$  [ $\sim 4 \times 10^{11} B$  (Hz/T) for  $(\text{Per})_2\text{Au}(\text{mnt})_2$ ] is the frequency at which the carriers are swept across the Fermi surface sheets in the first Brillouin zone. Hence the field and temperature dependence the transmission of the oscillatory QI amplitude is  $A_{\text{QI}} \sim -2pq \cos(\Psi) \exp[-\pi/\omega_c\tau(T)]$ .

Comparing the magnetic field dependence, the amplitudes of the MR oscillations for LQ would grow exponentially with increasing fields whereas for QI they are limited by the envelope term  $pq \exp(-\pi/\omega_c\tau)$ . Although the MR oscillations associated with the QI behavior are periodic in inverse field, there is no direct correspondence between the quantum limit for LQ (i.e.,  $E = \hbar\omega_c(n + \frac{1}{2})$  where  $n \rightarrow 0$ ) and the high-field limit for QI (in this case 20 T) where  $\Psi \rightarrow 0$ .

In Fig. 4 the field direction dependence of the MR is shown for  $(\text{Per})_2\text{Au}(\text{mnt})_2$  (sample PA2) at 8.2 kbar. The angular dependence of the field positions of the QI oscillations exhibits an approximate  $1/\cos(\theta)$  relationship, shown explicitly for the  $N=2$  dip in Fig. 4(b). In addition to the single fundamental frequency  $F_0$ , a higher harmonic ( $2F_0$ ) appears and a variation in the harmonic amplitude ratio with angle is evident. However, we find no direct correspondence with the LK angular dependence for LQ behavior, where for a Q2D cylindrical topology the ratio  $R_S(1)/R_S(2)$  oscillates dramatically in a symmetric manner<sup>27</sup> around  $\theta=0$ . The higher-harmonic contributions seen in Fig. 4 are expected from QI when more than one Brillouin zone is traversed before interference takes place. Moreover, the QI phase difference will be sensitive to the plane of the orbits (i.e., field direction) with respect to the Fermi surface topology.<sup>25</sup>

The estimated frequency  $F_0$  of QI effect is determined from the relationship<sup>25</sup>  $\Psi = \hbar A_k/eB = 2\pi F_0/B$ , where  $A_k$  is the extremal area enclosed by the two trajectories in  $k$  space. From Fig. 1,  $A_k \sim 2\delta k_a$ , which yields  $F_0 \sim 24$  T, neglecting additional warping of the sheets. The predicted frequency is in good agreement with the measured frequency  $F_0 \sim 20$  T. By inspection of Figs. 2 and 4, the oscillatory amplitudes do not grow exponentially as  $R_D$  in field, but saturate above 10 T. The term  $A_{\text{QI}}$  is shown in the inset of Fig. 2(b) for constant temperature. This simple model captures the field dependence of the oscillatory data and also defines the indexing scheme in terms of constructive and destructive interference where  $N=1$  appears near 20 T.

The open-orbit FS topology of Fig. 1(a) clearly favors the QI effect, since it is unlikely that pressure could connect FS sections over  $2k_F$  to form Q2D closed orbits. Moreover, if small electron and hole pockets resulted from imperfect (including field-induced) nesting of the 1D sheets, the extremal areas of such pockets would be significantly less than the area  $A_k$  between the warped 1D FS sheets. We find no evidence for oscillations with frequencies lower than  $\sim 20$  T in our data. Field-induced subphases, as seen in the TMTSF-based salts, have temperature-dependent threshold fields  $H_{\text{th}}$  with a pronounced hysteresis.<sup>11</sup> In comparison, the location of the low-field MR peaks observed for  $(\text{Per})_2\text{Au}(\text{mnt})_2$  under pressure is nearly temperature independent and no hysteresis has been observed. Likewise, Hall-effect measurements (not shown) exhibit no evidence for Hall quantization, as is seen in other quasi-two-dimensional bulk materials.<sup>28–31</sup> The absence of Hall quantization in  $(\text{Per})_2\text{Au}(\text{mnt})_2$  is consistent with the QI effect, since there is no Landau gap to pin the Fermi level.

The temperature dependence of the  $B=0$  resistivity for sample PA2 at 5.0 kbar is shown in the inset of Fig. 5(a). In agreement with the previous work in Ref. 16, we find that the resistance is generally sublinear in temperature above a characteristic temperature  $T_{\text{min}}$  and weakly activated below  $T_{\text{min}}$ . In the pressure regime above  $P_c \sim 5$  kbar, the  $d[\ln(R)]/d(1/T)$  peak associated with  $T_{\text{CDW}}$  (Ref. 17) is already suppressed. The temperature dependence of the MR oscillation amplitudes for the 5.0 kbar data is shown in Fig. 5(a). We have taken the peak-to-valley amplitude difference for oscillations in the 10–20 T range and normalized the difference by the nonoscillatory background MR below 2 T. For comparison, we show the temperature dependence at constant field predicted by  $\exp[-\pi/\omega_c\tau(T)]$  and the LK damping factor  $R_T R_D$  where in both terms we assume  $\tau(T) \propto T^{-2}$  from Fermi-liquid behavior (i.e.,  $\rho \sim T^2$ ) and an effective mass  $= 1m_e$ . It is important to note in Fig. 5(a) that from (i) and (ii) above,  $R_D$  and  $A_{\text{QI}}$  are both proportional to  $\exp[-1/\tau(T)]$ .

By inspection, Fig. 5(a) shows that in no case can the Fermi-liquid term  $\tau(T) \sim T^{-2}$  account for the analytic form (upwards curvature) of the oscillation-amplitude temperature dependence. Moreover, the LK factor  $R_T R_D$  becomes negligible at 4 K, but experimentally, oscillations are observable even above 10 K. In contrast, for a weakly temperature-independent  $\tau(T)$ , the oscillations associated with QI will

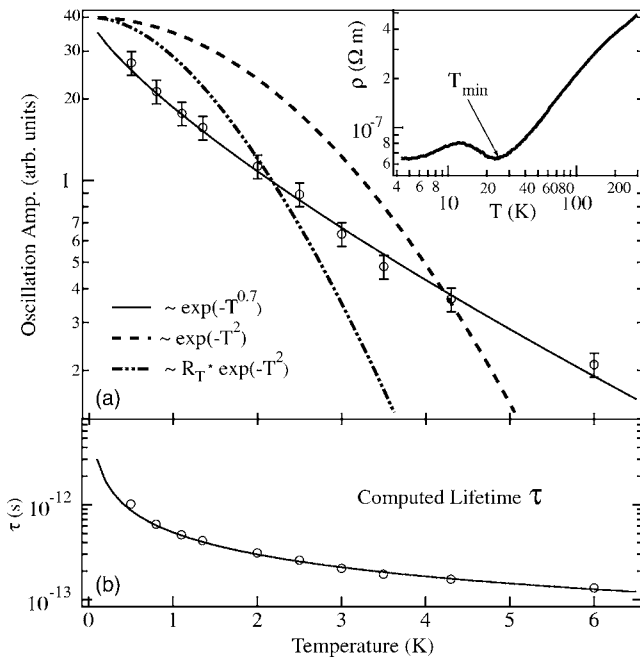


FIG. 5. Temperature-dependent parameters of  $(\text{Per})_2\text{Au}(\text{mnt})_2$  (sample PA2) for 5.0 kbar. (a) Oscillatory amplitudes in the range 10–20 T normalized by the background MR for 5.0 kbar. The solid line corresponds to a computed amplitude from QI theory where  $\tau \sim T^{-0.77}$  is obtained from (b). The data and calculated values agree within 10%, shown by the error bars. The dashed line represents the LK factor  $R_D$  with a Fermi-liquid ( $\rho \sim T^2$ ) temperature dependence and scattering rate ( $\tau \sim T^{-2}$ ). The dash-dotted line corresponds to the same dependence modified by  $R_T$  with  $m_c=1$  (i.e.,  $R_T R_D$ ). Inset: temperature dependence of the resistivity, where  $T_{\min}$  is the characteristic minimum resistivity temperature (Ref. 16). (b) The computed QI lifetimes based on the experimental data in 5(a). The solid curve is a  $\tau \sim T^{-0.77}$  fit to the data.

occur over a much broader temperature range.<sup>14</sup> Normally,  $\tau$  can be estimated from the (zero-field) temperature dependence of the resistivity<sup>10,14</sup> using the simple relation  $\rho(T) = m^*/ne^2\tau(T)$ . But here the low-temperature resistivity under pressure is complicated by the presence of the CDW ground state, and even for pressures above the critical pressure  $P_c$  where  $T_{\text{CDW}}$  disappears,<sup>16</sup> the resistivity does not

show  $\rho \sim T^2$  behavior below  $T_{\min}$ . This anomalous behavior in CDW systems under pressure has been described as a “quantum melting” where CDW fluctuations still are present, but with no long-range order.<sup>16,32</sup> Therefore the coexistence of separated metallic and nonmetallic regimes can lead to an anomalous  $\tau(T)$  behavior. Since the oscillatory MR behavior will be connected with the metallic phase, we have fit the expression  $A_{\text{QI}} \sim \exp(-\pi/\omega_c\tau)$  to determine  $\tau(T)$  from the experimental data, as shown in Fig. 5(b). We find that  $\tau(T) \sim T^{-\gamma}$  where  $\gamma$  is in the range  $0.6 < \gamma < 0.8$ . This corresponds to a sublinear dependence of the metallic phase resistivity on temperature and accounts for the temperature dependence of the oscillation amplitudes. Recently, the organic CDW system TTF-TCNQ, measured under pressure, was found to have a similar temperature dependence with  $\rho \sim T^{0.76}$ .<sup>33</sup>

In summary, the oscillatory MR behavior in pressurized  $(\text{Per})_2\text{Au}(\text{mnt})_2$  arises from quantum interference between nearly one-dimensional carrier trajectories. Above 20 T, the constructive interference limit is approached, where the phase difference between trajectories goes to zero. We find consistency between the Fermi surface topology derived from the QI data and the details of the band-structure calculation. The temperature dependence of the QI amplitudes for pressurized  $(\text{Per})_2\text{Au}(\text{mnt})_2$  is analytically different than in other materials with purely metallic ground states.<sup>9,10,14</sup> Using the QI model, where the attenuation factor is  $\exp(-1/\tau)$ , we can satisfactorily fit the oscillation amplitude data in Fig. 5(a) and obtain an expression for the anomalous carrier scattering time. Our results support the existence of an inhomogeneous ground state in pressurized  $(\text{Per})_2\text{Au}(\text{mnt})_2$  at low temperatures where mesoscopic metallic and nonmetallic regions coexist.

#### ACKNOWLEDGMENTS

We would like to acknowledge support from Grants Nos. NSF-DMR 0203532 and 0602859 and FCT (Portugal) under Contract No. POCT/FAT/39115/2001. The experimental portion of this work was performed at the National High Magnetic Field Laboratory, which is supported by NSF Cooperative Agreement No. DMR-0084173, by the State of Florida, and by the DOE.

<sup>1</sup>C. Davisson and L. H. Germer, *Phys. Rev.* **30**, 705 (1927).

<sup>2</sup>G. Mollenstedt and H. Duker, *Z. Phys.* **145**, 377 (1956).

<sup>3</sup>C. Jönsson, *Z. Phys.* **161**, 454 (1961).

<sup>4</sup>Y. Aharonov and D. Bohm, *Phys. Rev.* **115**, 485 (1959).

<sup>5</sup>R. G. Chambers, *Phys. Rev. Lett.* **5**, 3 (1960).

<sup>6</sup>S. Olariu and I. I. Popescu, *Rev. Mod. Phys.* **57**, 339 (1985).

<sup>7</sup>R. W. Stark and C. B. Friedberg, *Phys. Rev. Lett.* **26**, 556 (1971).

<sup>8</sup>N. B. Sandesara and R. W. Stark, *Phys. Rev. Lett.* **53**, 1681 (1984).

<sup>9</sup>C. Proust, A. Audouard, L. Brossard, S. Pesotskii, R. Lyubovskii, and R. Lyubovskaya, *Phys. Rev. B* **65**, 155106 (2002).

<sup>10</sup>N. Harrison, R. G. Goodrich, J. J. Vuillemin, Z. Fisk, and D. G.

Rickel, *Phys. Rev. Lett.* **80**, 4498 (1998).

<sup>11</sup>T. Ishiguro, K. Yamaji, and G. Saito, *Organic Superconductors II* (Springer-Verlag, Berlin, 1998).

<sup>12</sup>H. Schwenk, S. S. P. Parkin, R. Schumaker, R. L. Greene, and D. Schweitzer, *Phys. Rev. Lett.* **56**, 667 (1986).

<sup>13</sup>X. Yan, M. J. Naughton, R. V. Chamberlin, S. Y. Hsu, L. Y. Chiang, J. S. Brooks, and P. M. Chaikin, *Phys. Rev. B* **36**, 1799 (1987).

<sup>14</sup>S. Uji, T. Terashima, H. Aoki, J. S. Brooks, M. Tokumoto, S. Takasaki, J. Yamada, and H. Anzai, *Phys. Rev. B* **53**, 14399 (1996).

<sup>15</sup>M. Almeida and R. T. Henriques, in *Handbook of Organic Con-*

- ductive Molecules and Polymers*, edited by H. Nalwa (Wiley, New York, 1997), Vol. 1, p. 87.
- <sup>16</sup>N. Mitsu, K. Yamaya, M. Almeida, and R. T. Henriques, *J. Phys. Chem. Solids* **66**, 1567 (2005).
- <sup>17</sup>D. Graf, J. S. Brooks, E. S. Choi, S. Uji, J. C. Dias, M. Almeida, and M. Matos, *Phys. Rev. B* **69**, 125113 (2004).
- <sup>18</sup>D. Graf, E. S. Choi, J. S. Brooks, R. T. Henriques, M. Almeida, and M. Matos, *Phys. Rev. Lett.* **93**, 076406 (2004).
- <sup>19</sup>E. Canadell, M. Almeida, and J. S. Brooks, *Eur. Phys. J. B* **42**, R453 (2004).
- <sup>20</sup>L. Alcacer and A. H. Maki, *J. Phys. Chem.* **78**, 215 (1974).
- <sup>21</sup>E. B. Lopes, M. J. Matos, R. T. Henriques, M. Almeida, and J. Dumas, *Europhys. Lett.* **27**, 241 (1994). Analysis of the currents used in this experiment show that the electric fields produced did not exceed the threshold electric fields measured in Ref. [21](#) at ambient pressure ( $E_{\text{th}} \sim 400$  mV/cm) or in Ref. [16](#) ( $E_{\text{th}} \sim 30$  mV/cm) at 16 kbar. Therefore nonlinear effects were not a factor in our measurements.
- <sup>22</sup>R. McDonald, N. Harrison, L. Balicas, K. H. Kim, J. Singleton, and X. Chi, *Phys. Rev. Lett.* **93**, 076405 (2004).
- <sup>23</sup>R. D. McDonald, N. Harrison, J. Singleton, A. Bangura, P. A. Goddard, A. P. Ramirez, and X. Chi, *Phys. Rev. Lett.* **94**, 106404 (2005).
- <sup>24</sup>K. Murata, H. Yoshino, H. O. Yadav, Y. Honda, and N. Shirakawa, *Rev. Sci. Instrum.* **68**, 2490 (1997).
- <sup>25</sup>D. Shoenberg, *Magnetic Oscillations in Metals* (Cambridge University Press, Cambridge, England, 1994).
- <sup>26</sup>R. B. Dingle, *Proc. R. Soc. London, Ser. A* **211**, 500 (1952).
- <sup>27</sup>J. Wosnitza, G. W. Crabtree, H. H. Wang, U. Geiser, J. M. Williams, and K. D. Carlson, *Phys. Rev. B* **45**, 3018 (1992).
- <sup>28</sup>S. T. Hannahs, J. S. Brooks, W. Kang, L. Y. Chiang, and P. M. Chaikin, *Phys. Rev. Lett.* **63**, 1988 (1989).
- <sup>29</sup>J. R. Cooper, W. Kang, P. Auban, G. Montambaux, D. Jerome, and K. Bechgaard, *Phys. Rev. Lett.* **63**, 1984 (1989).
- <sup>30</sup>S. Hill, S. Valfells, S. Uji, J. S. Brooks, G. J. Athas, P. S. Sandhu, J. Sarrao, Z. Fisk, and J. Goettee, *Phys. Rev. B* **55**, 2018 (1997).
- <sup>31</sup>K. Murata, T. Nakanishi, H. Yoshino, T. Konoike, J. S. Brooks, D. Graf, and G. C. Papavassiliou, *J. Phys. IV* **114**, 343 (2004).
- <sup>32</sup>C. S. Snow, J. F. Karpus, S. L. Cooper, T. E. Kidd, and T. C. Chiang, *Phys. Rev. Lett.* **91**, 136402 (2003).
- <sup>33</sup>S. Yasuzuka, K. Murata, T. Arimoto, and R. Kato, *J. Phys. Soc. Jpn.* **76**, 033701 (2007).